

On *FEM* modeling of piezoelectric actuators and sensors for thin-walled structures

Dragan Marinković^{*,1,2} and Zoran Marinković²

¹*Institute of Mechanics, Berlin Institute of Technology, Germany*

²*Faculty of Mechanical Engineering, University of Niš, Serbia*

(Received September 16, 2011, Revised March 25, 2012, Accepted April 2, 2012)

Abstract. Thin-walled adaptive structures render a large and important group of adaptive structures. Typical material system used for them is a composite laminate that includes piezoelectric material based sensors and actuators. The piezoelectric active elements are in the form of thin patches bonded onto or embedded into the structure. Among different types of patches, the paper considers those polarized in the thickness direction. The finite element method (*FEM*) imposed itself as an essential technical support for the needs of structural design. This paper gives a brief description of a developed shell type finite element for active/adaptive thin-walled structures and the element is, furthermore, used as a tool to consider the aspect of mesh distortion over the surface of actuators and sensors. The aspect is of significance for simulation of behavior of adaptive structures and implementation of control algorithms.

Keywords: thin-walled adaptive structures; piezoelectric actuators and sensors; *FEM*; mesh distortion

1. Introduction

A synergic integration of structures, multi-functional material based sensors and actuators and control electronics has redefined the concept of structures from a conventional passive elastic system to an adaptive controllable system with inherent self-sensing, diagnosis, control and actuation capabilities. Such integration enables the structure to respond in real time or nearly real time to external stimuli to compensate for undesired behavior or to produce a desired response through the change of the structure's stiffness, inertial properties, damping properties or configuration.

The attractiveness of the new emerged field of adaptive structures stems from the already exploited as well as potential benefits they offer with respect to classical, passive structures (Gandhi *et al.* 1992), such as vibration suppression, noise attenuation, structural health monitoring (Lu *et al.* 2010), shape or position control (Rudolf *et al.* 2010), etc. The development and design of adaptive structures requires reliable, accurate and numerically efficient tools for modeling and simulation. The finite element method (*FEM*), as the predominant one in the field of structural analysis, is almost inevitably addressed on the matter. The body of literature considering the finite element approach to modeling piezoelectric based active/adaptive thin-walled structures is quite large. A survey such as one from Benjeddou (2000) gives an overview of the development in the field during the '90s. And the development proceeded at the same rapid pace in the decade to follow.

*Corresponding author, Assistant professor, E-mail: Dragan.Marinkovic@TU-Berlin.de

A reliable simulation is supposed to provide an easier, faster and less expensive development of adaptive structures, needed active elements and control algorithms. Realization of such a simulation requires, furthermore, reliable and accurate prediction of signals and loads produced by sensors and actuators, respectively. This paper is turned to the aspect of *FE* mesh distortion over the area of piezoelectric actuators and sensors. A number of authors have so far considered their finite elements with respect to the matter demonstrating robustness and potential benefits their development offered compared to already existing finite elements. Various techniques have been applied to achieve both, alleviate locking phenomena and improve the results for distorted *FE*-meshes. Among them are addition of bubble/incompatible modes (Tzou *et al.* 1990) discrete shear gap and assumed natural strain approach (Zemcik *et al.* 2006), selectively (Lamering 1991) and uniformly (Marinkovic *et al.* 2006) reduced integration, mixed interpolation of tensorial components (Klinkel *et al.* 2006), etc. Some authors pointed out that the solutions based on hybrid formulations are less sensitive to mesh distortion (Sze *et al.* 1999, Long *et al.* 2006). Another group of authors sought the solution for mesh distortion related problems in mesh-free formulations, such as meshless point collocation method (Ohs *et al.* 2001), point interpolation method (Liu *et al.* 2002), radial point interpolation method (Liu *et al.* 2003) or stabilized conforming nodal integration mesh-free method (Nguyen-Van *et al.* 2008). Some approaches combine the displacement-based *FEM* formulation with the strain smoothing technique of mesh-free methods to produce the smoothed finite element method, whereby the smoothing technique is developed based on the Hu-Washizu three-field variational principle (Liu *et al.* 2007). All these efforts demonstrate the interest of the research community to improve various aspects related to *FEM*-modeling of adaptive structures, the mesh distortion being one of them.

A vast majority of commercially available *FEM* software packages utilize the displacement-based *FEM* formulation and the focus of the paper is, therefore, on this formulation. In the case of electro-mechanical coupling, this means that mechanical displacements and electric voltages are the degrees of freedom. The authors of the paper do not intent to offer a new technique to mitigate the consequences of mesh distortion. They rather tend to give an insight about the influence of mesh distortion, when it affects a part of the structure characterized by electro-mechanical coupling and modeled by means of displacement-based *FEM*. To the best of the authors' knowledge, the available literature in the field does not offer such an insight. For this purpose, an already developed shell type finite element (Marinkovic 2007) is used. For the sake of completeness, the element is briefly presented in the paper. The insight is supposed to give hints as to how the mesh distortion over the piezoelectric active elements affects the resulting sensor signals and induced deformations, when the displacement-based *FEM* formulation is used in modeling. Additionally, the effect of the already known technique based on uniformly reduced integration, in combination with the presented shell type element, is demonstrated in one of the considered cases, in which the deterioration of accuracy caused by mesh distortion has imposed the need for further investigation.

2. A brief description of the active composite shell element

The geometry of a generally shaped thin-walled structure is typically described as a shell. Among different approaches to finite element modeling of shell type structures, the degenerate shell approach belongs to the group of most appealing formulations. The degenerate shell element was first developed by Ahmad *et al.* (1970) from a 3D solid element by a "degeneration process", which directly reduced the 3D field approach to a 2D one in terms of mid-surface nodal variables. The

most significant advantages achieved in this manner are that the element is not based on the classical shell theories and is applicable over a wide range of thickness and curvatures. The developed element, referred to as *ACShell9* (9-node active composite shell), represents the extension to modeling active multi-layered structures made of fiber-reinforced composites and including active piezoelectric layers polarized in the thickness direction. Only a brief description of the element formulation will be given here and for more details an interested reader is referred to (Marinkovic 2007).

2.1 Geometry and mechanical field of the element

The inherent complexity of the degenerate shell element requires the usage of several coordinate systems in order to describe the element geometry, displacement field and to develop the strain field (Fig. 1). Besides the global (x, y, z) and the natural (r, s, t) coordinate system (*c.s.*) it is necessary to introduce the local-running (co-rotational) coordinate system (x', y', z') . The local coordinate system is defined so as to have one of its axes (say z' -axis) perpendicular to the mid-surface, while the other two axes form the tangential plane. Furthermore, if the basic structural material is a fiber-reinforced composite laminate, the kind of non-isotropy exhibited by such a material requires introduction of a structure reference direction (defined by the user), with respect to which the fiber orientation in the layers is given. In this case it is reasonable to fix the orientation of the local in-plane axes with respect to the structure reference direction. The simplest way is overlapping one of the axes (say the x -axis) with it. This allows direct application of the composite laminate constitutive law, i.e., the well-known *ABD* matrix.

Using the full biquadratic Lagrange shape functions N_i , the coordinates of a reference-surface point are

$$\{x \ y \ z\}^T = \sum_{i=1}^9 N_i \{x_i \ y_i \ z_i\}^T \tag{1}$$

with x_i, y_i and z_i denoting global coordinates of the nine nodes. The thickness of the shell is assumed to be in the direction normal to the reference-surface and denoting the unity vector in the thickness direction as $\vec{e}_{z'i}$ the 3D shell geometry may be given as

$$\{x \ y \ z\}^T = \sum_{i=1}^9 N_i \{x_i \ y_i \ z_i\}^T + \sum_{i=1}^9 \frac{h_i}{2} N_i t \vec{e}_{z'i} \tag{2}$$

where h_i is the shell thickness at node i and t is the natural counterpart of the local thickness coordinate.

The degeneration process is based on the assumption that the thickness direction line of the shell remains straight after deformation but not necessarily perpendicular to the reference-surface (the

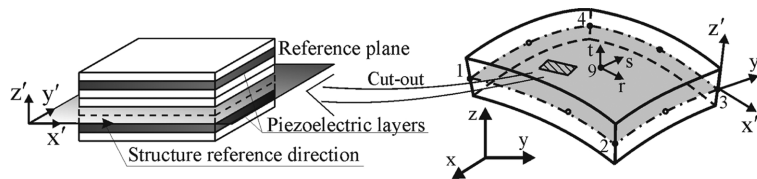


Fig. 1 Element geometry and coordinate systems

Mindlin kinematical assumption). Therefore, the displacement of any point within the volume of the shell is given as a superposition of the corresponding reference-surface point displacement and a linear function of the rotations about the local x' - and y' -axis through the mid-surface point, $\theta_{x'}$ and $\theta_{y'}$

$$\{u \ v \ w\}^T = \sum_{i=1}^9 N_i \{u_i \ v_i \ w_i\}^T + \sum_{i=1}^9 \frac{h_i}{2} N_i t [-\vec{e}_{y'i} \ \vec{e}_{x'i}] \{\theta_{x'} \ \theta_{y'}\}^T \quad (3)$$

The rotations are in the local c. s. and upon transformation to the global c. s. one gets:

$$\{u \ v \ w\}^T = \sum_{i=1}^9 N_i \{u_i \ v_i \ w_i\}^T + \sum_{i=1}^9 \frac{h_i}{2} N_i t [-\vec{e}_{y'i} \ \vec{e}_{x'i}] [T']^T \{\theta_x \ \theta_y \ \theta_z\}^T \quad (4)$$

where $[T']$ is the modified form of the transformation matrix relating the local and the global coordinate system, $[T]$, and is given in the form $[T'] = [\vec{e}_{x'} \ \vec{e}_{y'}]$.

Due to the directionally dependent material properties, it is of crucial importance to develop the strain field in the local coordinate system (Fig. 2). This allows direct application of the composite laminates constitutive (ABD) matrix. The advantage of having the strain field with respect to the local coordinate system is also obvious when the piezoelectric coupling within the thickness-polarized piezopatch operating on the “ e_{31} -effect” is considered. The development of the strain field with respect to the local c.s. is done in several steps. The interpolations are performed in the natural c.s. Hence, the displacement derivatives with respect to the natural coordinates are directly obtained from Eq. (4). The transformation of derivatives from the natural to the global coordinate system is achieved by means of Jacobian inverse

$$[J] = \begin{bmatrix} x_{,r} & y_{,r} & z_{,r} \\ x_{,s} & y_{,s} & z_{,s} \\ x_{,t} & y_{,t} & z_{,t} \end{bmatrix} \Rightarrow \begin{bmatrix} u_{,x} & v_{,x} & w_{,x} \\ u_{,y} & v_{,y} & w_{,y} \\ u_{,z} & v_{,z} & w_{,z} \end{bmatrix} = [J]^{-1} \begin{bmatrix} u_{,r} & v_{,r} & w_{,r} \\ u_{,s} & v_{,s} & w_{,s} \\ u_{,t} & v_{,t} & w_{,t} \end{bmatrix} \quad (5)$$

where, for example, $u_{,xx} = \partial u / \partial x$. The global derivatives are afterwards transformed to the local derivatives by means of the transformation matrix $[T] = [\vec{e}_{x'} \ \vec{e}_{y'} \ \vec{e}_{z'}]$

$$\begin{bmatrix} u'_{,x'} & v'_{,x'} & w'_{,x'} \\ u'_{,y'} & v'_{,y'} & w'_{,y'} \\ u'_{,z'} & v'_{,z'} & w'_{,z'} \end{bmatrix} = [T]^T \begin{bmatrix} u_{,x} & v_{,x} & w_{,x} \\ u_{,y} & v_{,y} & w_{,y} \\ u_{,z} & v_{,z} & w_{,z} \end{bmatrix} [T] \quad (6)$$

It is quite common within a 2D formulation to give the strain field in the form that makes a distinction between the in-plane components and the out-of-plane strain components

$$\{\mathcal{E}'\} = \{\mathcal{E}'_{x'x'} \ \mathcal{E}'_{y'y'} \ \gamma'_{x'y'} \mid \gamma'_{y'z'} \ \gamma'_{x'z'}\}^T$$

i.e.

$$\{\mathcal{E}'\} = \{u'_{,x'} \ v'_{,y'} \ u'_{,y'} + v'_{,x'} \mid v'_{,z'} + w'_{,y'} \ u'_{,z'} + w'_{,x'}\}^T \quad (7)$$

After determining the partial derivatives in the local coordinate system (Eq. (6)), the strain field is

given in the following form

$$\{\varepsilon'\} = \begin{Bmatrix} \{\varepsilon'_{mf}\} \\ \{\varepsilon'_s\} \end{Bmatrix} = \begin{bmatrix} [B_{mf}] \\ [B_s] \end{bmatrix} \{d\} = \begin{bmatrix} [B_{Tm}] & | & t[B_{R1f}] \\ [B_{Ts}] & | & [B_{R0s}] + t[B_{R1s}] \end{bmatrix} \{d\} = [B_u] \{d\} \quad (8)$$

where $\{\varepsilon'_{mf}\}$ is the membrane-flexural (in-plane) strain field, $\{\varepsilon'_s\}$ comprises transverse shear strains, $[B_{mf}]$ and $[B_s]$ are the corresponding strain-displacement matrices further suitably represented in terms of the B -matrices having “ m ”, “ f ” and “ s ” in the subscript depending whether they contribute to the definition of the membrane, flexural or shear strains, respectively, those having “ T ” are related to the nodal translations and with “ R ” are related to the nodal rotations, and finally, “ 0 ” denotes constant terms while “ 1 ” denotes linear terms with respect to the natural thickness coordinate t . The mentioned matrices render together the strain-displacement matrix $[B_u]$. The vector $\{u\}$ comprises nodal mechanical displacements (translations and rotations).

2.1 Piezoelectric layer

The constitutive equations of the piezoelectric material depend on the choice of independent variables. Since in the displacement-based *FEM* formulation mechanical displacements and electric voltages are the degrees of freedom, it is convenient to take the form of the piezoelectric constitutive equations that corresponds to the choice of mechanical strain and electric field as independent variables, so that

$$\begin{aligned} \{\sigma\} &= [C^E] \{\varepsilon\} - [e] \{E\} \\ \{D\} &= [e] \{\varepsilon\} + [d^E] \{E\} \end{aligned} \quad (9)$$

where $\{\sigma\}$ is the mechanical stress in vector (Voigt) notation, $\{D\}$ is the electric displacement vector, $[C^E]$ is the piezoelectric material Hook's matrix at constant electric field E , $[d^E]$ is the dielectric permittivity matrix at e constant, and $[e]$ is the piezoelectric coupling matrix.

This paper considers active piezoceramic elements with electrodes on the top and bottom surfaces and poled in the thickness direction, where the in-plane strains are coupled to the perpendicularly applied electric field through the piezoelectric “ e_{31} -effect”. An investigation about the accurate description of the electric potential distribution across the thickness of the piezolayer (Marinkovic *et al.* 2007, Marinkovic *et al.* 2009) demonstrated that the consistent functions depend on the applied 2D-theory for modeling thin-walled structures. The investigation also demonstrated that, although a linear distribution of the electric potential and the corresponding constant electric field are only approximations of the actual functions when a first-order 2D theory is used (in that case, a quadratic interpolation of electric potential through the thickness yields the correct result (Benjedou *et al.* 2002)), they are still accurate enough for the purpose of modeling global structural behavior. Thus, they are adopted here

$$E = -\frac{\partial \varphi}{\partial z'} \Rightarrow E_k = \frac{\Delta \Phi_k}{h_k} \quad (10)$$

where φ is the electric potential, $\Delta \Phi_k$ is the difference of electric potentials between the electrodes of the k^{th} layer and h_k is the thickness of the piezolayer. The approximation in Eq. (10) defines a diagonal electric field - electric potential matrix $[B_\phi]$ with typical term $1/h_k$ on the main diagonal. The diagonal

form of the matrix $[B_\phi]$ results from the fact that the difference of electric potentials of a layer directly affects only the electric field within the very same layer (of course, it also affects the electric field of other layers, but this “indirect” influence is described by the piezoelectric coupling).

3. Finite element equations

The finite element equations for dynamic behavior of piezoelectric continuum are obtained starting from the variational approach (Marinkovic 2007) and they are given in the following standard form

$$[M]\{\ddot{d}\} + [C]\{\dot{d}\} + [K_{uu}]\{d\} + [K_{u\phi}]\{\phi\} = \{F_{ext}\} \quad (11)$$

$$[K_{\phi u}]\{d\} + [K_{\phi\phi}]\{\phi\} = \{Q_{ext}\} \quad (12)$$

where the following matrices and vectors are introduced on the element level: the mass $[M]$, (proportional Rayleigh) damping $[C]$, mechanical stiffness $[K_{uu}]$, piezoelectric stiffness $[K_{u\phi}] = [K_{\phi u}]^T$ and dielectric stiffness $[K_{\phi\phi}]$ matrix as well as vectors of external forces $\{F_{ext}\}$ and electric charges $\{Q_{ext}\}$. Equations for a static case are easily obtained from the above given equations by excluding the inertia and damping terms. Since the rate of change of the electric field is much higher than the rate of change of the mechanical field, the inertial and damping effects are already neglected for the electric field. That is why Eq. (12) appears to be static. However, in dynamic or in nonlinear analysis, it is time dependent because it is coupled to Eq. (11). Thus the *FEM* equations for a static case read

$$[K_{uu}]\{d\} + [K_{u\phi}]\{\phi\} = \{F_{ext}\} \quad (13)$$

$$[K_{\phi u}]\{d\} + [K_{\phi\phi}]\{\phi\} = \{Q_{ext}\} \quad (14)$$

For further discussion, it is quite useful to give the expressions for the matrices in Eqs. (13) and (14)

$$[K_{uu}] = \int_{V_e} ([B_u]^T [C^E] [B_u]) dV \quad (15)$$

$$[K_{u\phi}] = \int_{V_e} ([B_u]^T [e]^T [B_\phi]) dV = [K_{\phi u}]^T \quad (16)$$

$$[K_{\phi\phi}] = - \int_V [B_\phi]^T [d^e] [B_\phi] dV \quad (17)$$

4. Aspect of mesh distortion over piezoelectric active patches

The output of piezoelectric sensors is electric voltage that reflects the average strain induced in the sensor patch, thus providing the information about the deformed state of the structure. On the other hand, the piezoelectric actuators use the inverse piezoelectric effect to induce mechanical loads with the aim of cancellation of undesired or causing desired deformations. The induced sensor signal is transferred to a controller that, based on the implemented control law, determines signals (electric voltages) for the actuators. Therefore, successful simulation of the behavior of adaptive

structures requires high accuracy in determining sensor signals and actuator loads.

It is a well-known fact that the mesh distortion of *FEM* models affects the accuracy of the obtained results. Regarding purely mechanical cases, the influence of mesh distortion upon the predicted structural behavior is known in general. A strict interpretation of the variational basis for the development of displacement type finite elements requires variationally correct solutions to have less energy than the exact solution (“boundedness”), meaning that *FEM* models yield stiffer behavior than the one exposed by the actual structures. The “stiffer behavior” becomes more pronounced for distorted meshes. In more practical words, the mesh distortion results in higher entries of the structure stiffness matrix, which is due to the higher values of entries in the strain-displacement matrix, $[B_u]$. Hence, it may be said that the mesh distortion results in a stiffer *FEM* model compared to the *FEM* model with undistorted mesh. However, regarding electromechanically coupled cases, the influence of mesh distortion becomes more complex. The piezoelectric stiffness matrix, $[K_{u\phi}]$, is also dependant on the strain-displacement matrix, $[B_u]$ and, hence, mesh distortion also causes larger entries in the piezoelectric coupling matrix. Nevertheless, the dependence of the mechanical stiffness matrix on the strain-displacement matrix is quadratic (Eq. (15)), whereas in the case of piezoelectric coupling matrix the dependence is linear (Eq. (16)). This combination of influences together with different applications of piezoelectric patches (sensors and actuators) and with a variety of possible boundary conditions makes the aspect worth of consideration.

For this purpose a rather simple structure that is well-known to the adaptive structures research community is used in the paper. It is the academic case of bimorph pointer, which has been exploited by a number of authors as a test case for developed numerical tools. The term “bimorph pointer” denotes a beam made of two uniaxial piezoelectric layers with opposite polarity and stacked together so that a bending actuator/sensor is obtained (Fig. 2). The device can be used for both micro-actuation and strain sensing. Due to the opposite polarization of the layers, the voltage applied across the thickness of the beam tends to induce strains in the layers of opposite signs. However, due to the fact that layers are bonded to each other, the strains are actually restraint and stresses are induced instead. The resultant of the stresses is a bending moment uniformly distributed over the edges of the beam. And, vice versa, if the beam is exposed to external mechanical excitation in the form of predefined displacement or a tip transverse force, it would deform and a voltage would be induced in the piezoelectric layers. The two oppositely polarized piezolayers amplify the effect resulting from the piezoelectric coupling and this is the reason why such a configuration is quite often used in many applications.

The considered example is originally proposed by Hwang *et al.* (1993). It is a bimorph piezoelectric

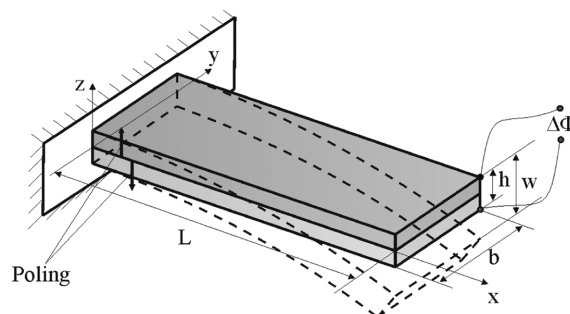


Fig. 2 Piezoelectric bimorph pointer

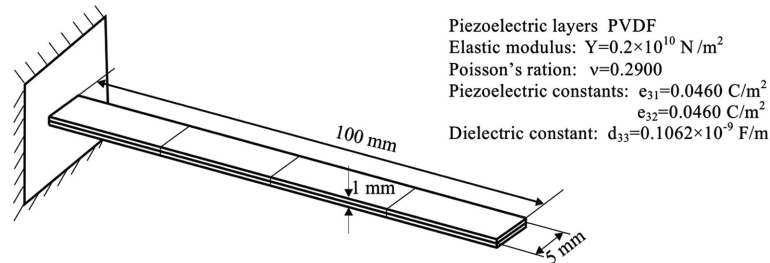


Fig. 3 Dimensions and material properties of the considered bimorph beam

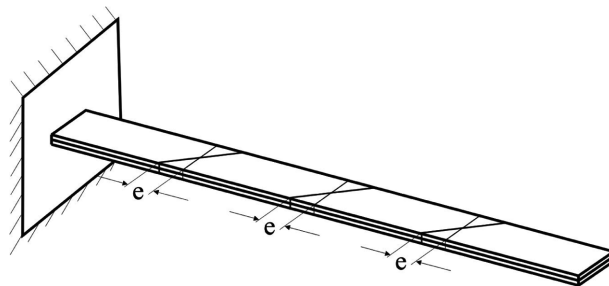


Fig. 4 Mesh distortion for the bimorph beam by varying parameter e

cantilever beam made of polyvinylidene fluoride (*PVDF*), the length of which is $L = 100 \text{ mm}$, the width $b = 5 \text{ mm}$ and the thickness $h = 1 \text{ mm}$. The geometry and material properties are given in Fig. 3 (all the material constants that are not specified are assumed to be equal to zero). It should be noted that *PVDF* is a rather compliant material and the contribution of the dead weight of the structure to the observed behavior would probably not be negligible. This effect is, however, neglected in the following examples, which only deepens their academic nature.

Discretization of the bimorph beam and a successive gradual mesh distortion are performed following the proposal by Sze *et al.* (1999). Hence, the original *FEM* model contains 4 identical elements along the beam length. The mesh distortion is realized according to Fig. 4 by increasing the parameter e in increments of 5 mm.

In the following, different excitations will be imposed onto the beam in order to consider the influence of described mesh distortion on the obtained results. Both actuator and sensor function of active layers are to be considered.

4.1 Actuator case - predefined voltage

First, the actuator function of piezoelectric layers is addressed. The predefined voltage of $\Delta\Phi = 1\text{V}$ is applied across the thickness of the beam, along the whole length. This is actually the original example proposed by Hwang *et al.* (1993) and then further used as a test case by a number of researchers, who developed *FE*-elements for modeling adaptive thin-walled structures.

The analytical solution for the deflection of the beam is obtained in a straight-forward manner. The bending moment induced through the inverse piezoelectric effect is calculated by integrating the normal stress component in the length direction (x -axis) over the cross-section (y - z plane)

$$M = \int_0^{b+h/2} \int_{-h/2}^0 \sigma_{xx} z \, dz \, dy + \int_0^b \int_{-h/2}^0 e_{31} E z \, dz \, dy + \int_0^{b+h/2} \int_0^0 e_{31} E z \, dz \, dy = \frac{bh^2}{4} e_{31} E \quad (18)$$

and the deflection is obtained as a quadratic function with respect to the x -coordinate, as follows

$$w = \frac{3e_{31}\Delta\Phi}{2Yh^2} x^2 \quad (19)$$

where Y denotes the Young's modulus and e_{31} is the piezoelectric constant that couples electric field in the thickness direction, E , to the stress component in the length direction. The analytical expression yields beam tip deflection of $3.45e-7$ m. It is interesting that already the model with only one *ACShell9* element along the length of the beam yields the analytical solution. The reason for this is the fact that the element uses full biquadratic shape functions and that the solution for the tip deflection is a quadratic function of the coordinate along the beam length (Eq. (19)).

Since the electric voltage is predefined, Eq. (14) is virtually excluded from the system of equations, which is then reduced to the following form

$$[K_{uu}]\{d\} = -[K_{u\phi}]\{\phi\} \quad (20)$$

As already elaborated, with the mesh distortion, the entries of both the mechanical stiffness matrix and the piezoelectric coupling matrix take higher values. Obviously, the mesh distortion affects the matrices on both sides of Eq. (20) in a similar manner. The *FEM*-model yields stiffer structure, but the bending moments due to the inverse piezoelectric effect are also computed as larger compared to the *FEM*-model with the undistorted mesh. Regarding the final result for mechanical displacements, it is to be expected that those two influences cancel each other up to a certain degree. Fig. 5 depicts the development of the normalized beam's free end deflection for successive mesh distortions as described above (parameter e taking values up to 20 mm). The normalization is done with respect to the same deflection computed with the undistorted mesh. The diagram confirms expectation, as the variation of the free end deflection computed with distorted meshes differs only slightly compared to the original result (undistorted mesh). In fact, the relative difference in result for all distorted meshes is fairly below 1%. The curve in Fig. 5 is quite similar in shape to the one reported by Sze *et al.* (1999) for a hybrid 8-node hexahedral finite element employing the selective scaling

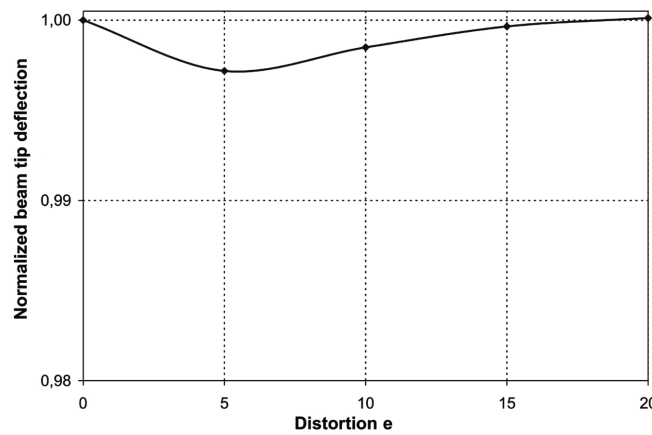


Fig. 5 Actuator case: normalized free end deflection

technique. Sze *et al.* (1999) report, however, noticeably larger relative differences, which may be attributed to the linear shape functions applied by their element. What is probably more interesting is the shape of the curve. For smaller values of parameter e , the normalized deflection decreases but for further mesh distortion it approaches slowly the original value of 1.0 and even exceeds it slightly for the parameter $e=20$ mm.

4.2 Sensor case

In practice, for the sensor function of piezolayers, the electrodes placed on the lower and the upper surface of the layers are short-circuited so that zero electric potential is enforced. The deformation caused by external mechanical loads results in electric displacement and thus electric charges are induced on the electrodes. Further on, either an electric charge amplifier or an electric current amplifier is used to determine the output voltage. In the former case, the output voltage is proportional to the average value of induced strains, while in the latter to the strain rate. In the following examples, this will be somewhat simplified. As a representative result, the electric voltage that would appear over the piezoelectric layers' electrodes is taken. Those are actually the electric degrees of freedom of the *FEM* model, which will be directly computed from the model.

As for the boundary conditions, the structure may be mechanically excited in two ways - by predefined forces and by predefined displacements. Although, from the mechanical point of view, there is no essential difference between the two, from the point of view of considered aspect (mesh distortion), it would be necessary to distinguish between the two in the case of piezoelectric structures, as it will be seen in the following. Furthermore, it is assumed that the whole bimorph beam is one sensor, since this allows investigation of influence of performed mesh distortion on the obtained results. This means that an additional condition is imposed in the model yielding that the electric voltage is same for all elements (considering one piezoelectric layer)

$$\phi_1 = \phi_2 = \dots = \phi_n \quad (20)$$

4.2.1 Sensor case - predefined force

In the first considered sensor case, a predefined transverse force is applied at the beam tip. The system of Eqs. (13) and (14) has now the following form:

$$[K_{uu}]\{d\} + [K_{u\phi}]\{\phi\} = \{F_{ext}\} \quad (21)$$

$$[K_{\phi u}]\{d\} + [K_{\phi\phi}]\{\phi\} = \{0\} \quad (22)$$

Compared to the previously considered case (i.e., the actuator case), the first difference to be noticed is that both Eqs. (13) and (14) are retained in the system of equations. Furthermore, the right-hand side of equations remains unaffected by mesh distortion, whereas both the mechanical stiffness and the piezoelectric coupling matrices are affected in the manner already discussed. The assembled dielectric stiffness matrix depends on the dielectric constant, thickness and surface of piezoelectric layers and its entries are, thus, not affected by the performed mesh distortion.

The sensor voltage induced by the beam tip transverse force is computed for different *FE*-meshes and the result is depicted in Fig. 6(a), where the normalization has been performed with respect to the *FE*-result yielded by the undistorted mesh ($e=0$). The obtained curve is very similar to the curve

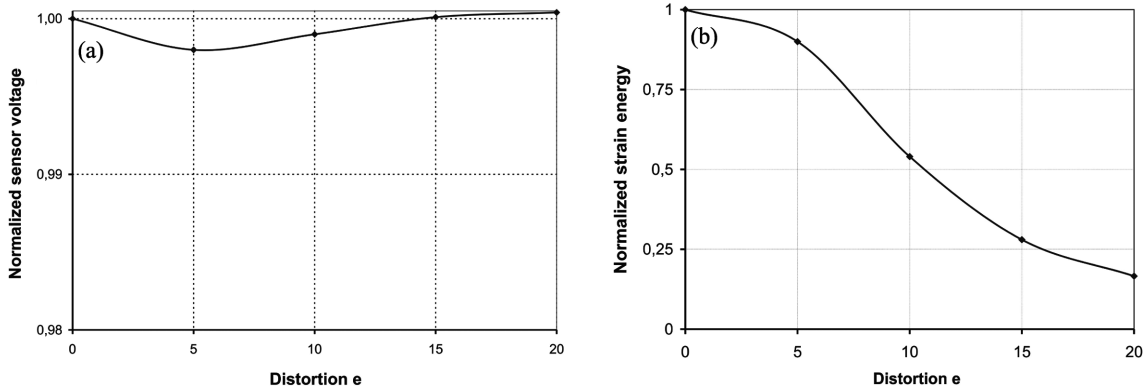


Fig. 6 Sensor case, predefined force: normalized sensor voltage and normalized strain energy

given in Fig. 5. This means that the influence of mesh distortion upon the mechanical stiffness matrix and the piezoelectric stiffness matrix once again cancel each other within the system of equations to a similar extent and, hence, the obtained result does not change dramatically. Since the electric voltage reflects the average strain in the sensor patch, in order to gain a better comprehension of the “canceling effect”, the change of the normalized strain energy is observed for the purely mechanical case (normalization done with respect to the result obtained for the initial *FE* mesh). The result is depicted in Fig. 6(b). As expected, the strain energy decreases as the mesh distortion progresses and the trend of the change is rather fast. Based on this result for the purely mechanical case, one would have expected that the computed normalized sensor signal in the piezoelectric case would also decrease with the progressing mesh distortion. However, as already elaborated, Fig. 6(a) reveals this is not the case and that is the consequence of the fact that the mesh distortion simultaneously affects both the mechanical stiffness and the piezoelectric coupling matrices in a similar manner.

4.2.2 Sensor case - predefined displacements

In this case, a predefined deflection of the beam tip is imposed as external excitation. This type of boundary condition is dealt with by determining external forces equivalent to the predefined displacements. The vector of nodal displacements can be divided into two vectors - $\{d^*\}$, which is completely known since it contains the predefined displacements at nodes where they are imposed and zeros at all other nodes, and $\{\bar{d}\}$, which contains unknown displacement at nodes other than those at which boundary conditions are defined and zeros at nodes with defined boundary conditions (predefined displacements or fixed boundary conditions), so that

$$\{d\} = \{d^*\} + \{\bar{d}\} \quad (23)$$

The system of Eqs. (13) and (14) can now be represented in the following form

$$[K_{uu}]\{\bar{d}\} + [K_{u\phi}]\{\phi\} = -[K_{uu}]\{d^*\} \quad (24)$$

$$[K_{\phi u}]\{\bar{d}\} + [K_{\phi\phi}]\{\phi\} = -[K_{\phi u}]\{d^*\} \quad (25)$$

The vectors on the right-hand side of the equations represent the equivalent external nodal

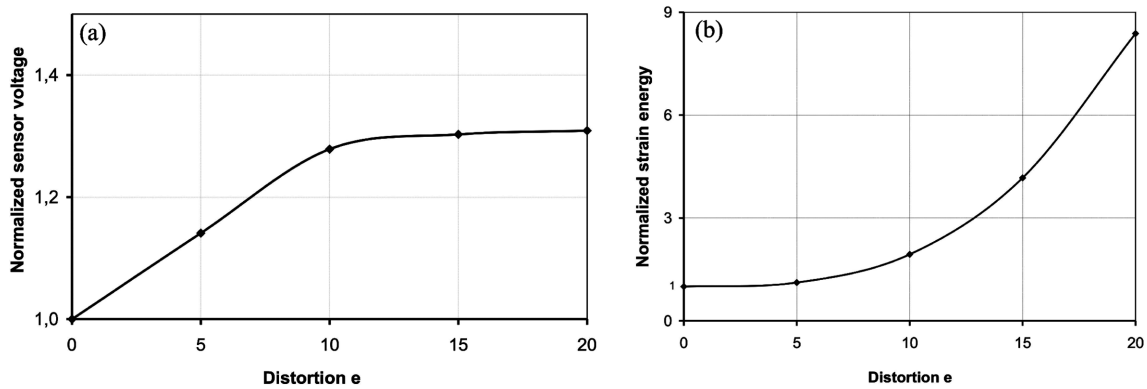


Fig. 7 Sensor case, predefined displacement: normalized sensor voltage and normalized strain energy

mechanical forces and electric charges that correspond to the predefined mechanical displacements. The obvious difference with respect to the previous case is that the right-hand side of the system of equations is dependant on mesh distortion. As the mesh distortion proceeds (parameter e takes higher values) the excitation equivalent to the predefined displacements increases.

The electric voltage has been again normalized with respect to the result obtained by undistorted mesh. The development of normalized electric voltage, depicted in Fig. 7(a), reveals a different tendency compared to the previous case that involves predefined forces. The computed sensor voltage increases with higher values of parameter e , thus reaching the value of approximately 1.3, which means that the sensor voltage, computed with the distorted mesh implementing the highest value of parameter e , is approximately 30% larger than the sensor voltage computed with the original (undistorted) mesh. If the same case is considered as a purely mechanical case, the strain energy increases rapidly as the mesh distortion progresses (Fig. 7(b)), which is the consequence of increasing equivalent forces on the right-hand side of Eq. (24) (piezoelectric coupling excluded), although the predefined displacements remain constant.

Hence, a significant sensitivity of computed sensor voltage to mesh distortion with predefined displacements as an excitation is noticed. This gave impetus to investigation if uniformly reduced integration technique (the 2×2 Gauss integration rule) could improve the result. Indeed, as Fig. 8

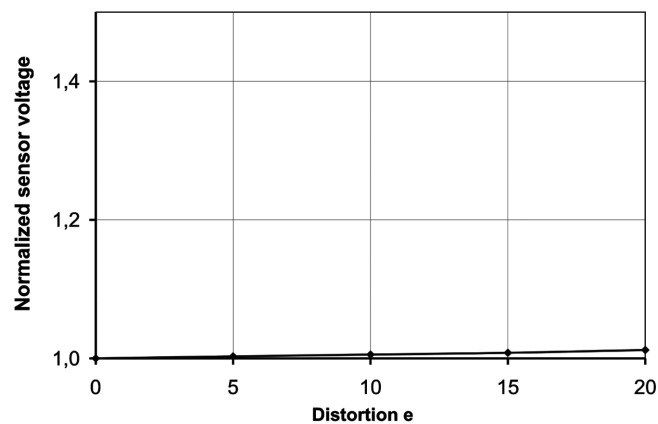


Fig. 8 Sensor case, predefined displacement: normalized sensor voltage with reduced integration technique

shows (the same scale used as in Fig. 7(a) for the purpose of comparison), the *ACShell9* element with the 2×2 integration rule yields remarkable improvement regarding the issue. The computed normalized voltage still takes higher values with the progressing mesh distortion, but the maximal increase is kept in reasonable limits (approximately 1.2% compared to 30% obtained with the full integration).

4.3 Actuator case - aspect of balance of induced loads

As already elaborated, electric voltage applied across the thickness of a collocated pair of oppositely polarized piezoelectric patches induces bending moments which are uniformly distributed over the edges of the surface covered by patches. If the patches are of rectangular shape, then the bending moments over the opposite sides of the rectangular surface covered by them are, in ideal case, balanced. Using a uniform mesh to discretize the surface yields balanced bending moments. The following example should illustrate the influence of mesh distortion on this aspect.

The example involves a beam made of aluminium, with two oppositely polarized piezoelectric patches made of *PIC151* bonded to the upper and lower beam surfaces so that they are collocated. The geometry and material properties are given in Fig. 9, with grey surface depicting the piezopatches. The patches are supplied with the same electric voltage, thus inducing actuating bending moments. With a uniform mesh, the computed bending moments are perfectly balanced over the opposite sides of the rectangular surface covered by the patches.

Mesh distortion has been done over the whole structure (Fig. 10), although it is the mesh distortion over the piezopatches that affects the results essentially. The mesh distortion has a twofold influence on the calculated bending moments. Firstly, they have higher values than in the case of the undistorted mesh - this effect has been already discussed. Additionally, the calculated bending moments over a pair of opposite (parallel) patch edges are not exactly balanced any more. Thus, the equilibrium of the structure as a whole is achieved by additional reaction moments acting at the support. Since the deflection of the beam tip has been observed, a simple way to investigate the impact of the unbalanced moments on the obtained result is to switch the calculated moments between the two parallel edges of the patches in the direction of the beam length (denoted as edges A and B in Fig. 10). In that case the difference in the obtained results directly indicates the “size of imbalance” of bending moments. The mentioned “switch” is simply performed by mirroring the part of the finite element mesh over the patches with respect to the axis of symmetry of the patches shown in Fig. 10 (mirror line). The result of the mirroring is that the bending moment distributed

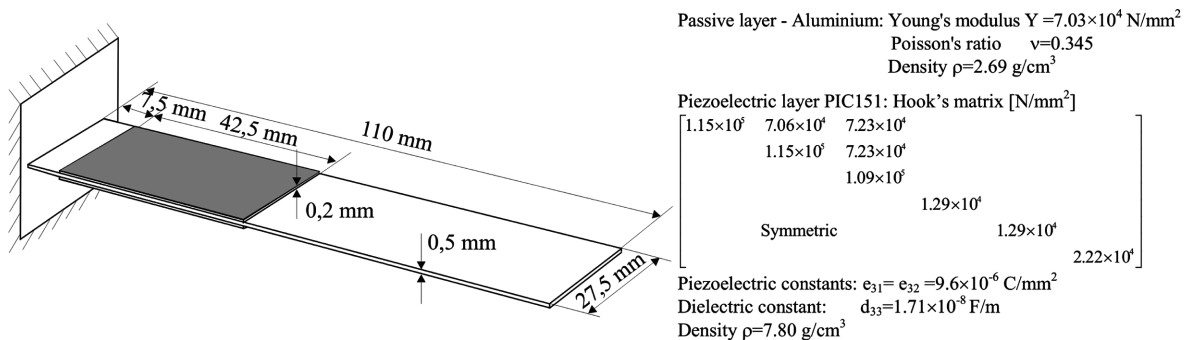


Fig. 9 Geometry and material properties of the active beam

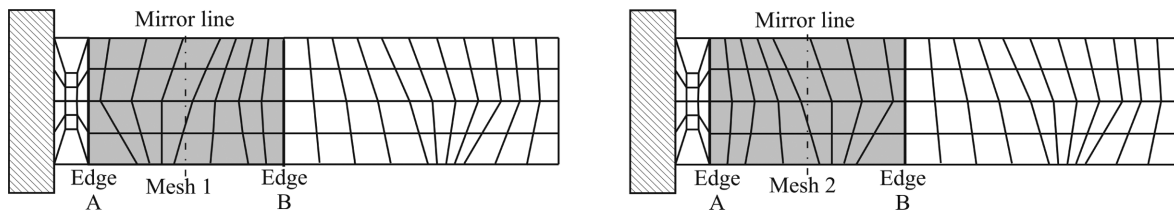


Fig. 10 The performed mesh distortion - mesh mirroring over the surface of piezoelectric actuators

over the edge A and calculated for the mesh 1 is the same as the bending moment distributed over the edge B for the mesh 2, only with opposite orientation (sign). A relatively small difference of 0.3% in the obtained results for the two distorted meshes is noticed. It was expected that the difference would not be large and it is to be attributed to the full biquadratic shape functions utilized by the element and the small distance between the clamped end of the beam and the piezopatches. This aspect, however, could be playing a more significant role with linear piezoelectric elements and differently shaped and supported active/adaptive structures.

5. Conclusions

The piezoelectric patches are frequently applied as active elements on thin-walled structures in order to obtain controllable dynamic response or static shape control of the structures. And the *FEM* has established itself as a standard method in structural analysis. That was the motivation for the authors to consider the aspect of *FE* mesh distortion over the surface covered by piezoelectric active elements.

Both actuator and sensor function of piezoelectric patches has been considered and the influence of *FE* mesh distortion over the surface of piezopatches onto the obtained results has been investigated. A recently developed and verified shell type finite element has been used in modeling. The considered examples involve simple structures with a relatively large surface covered by active elements, as it was aimed at rather obvious effects caused by mesh distortion. This enabled a straightforward assessment of the effect. It was shown that, in the case of coupled piezoelectric problems, the effect of mesh distortion is more complex compared to purely mechanical structural problems treated by means of *FEM*. Not only is the mechanical stiffness matrix affected by mesh distortion, but also is the piezoelectric coupling matrix. Furthermore, depending on the function of piezoelectric patches and predefined boundary conditions, the *FEM* system of equations takes different forms accordingly and the influence of mesh distortion gains even more on importance in certain cases. The actuator function (predefined voltages) and the sensor function of piezopatches with predefined mechanical loads appear to be less prone to mesh distortion. In those cases, the mesh distortion affects the mechanical stiffness and piezoelectric coupling matrices in such a manner so that those influences cancel each other within the system of equations leading to a final result that is not significantly altered compared to the result with a uniform *FE* mesh. However, the case of sensor function of piezopatches with predefined displacements imposed as external excitation has demonstrated much larger susceptibility to mesh distortion.

The comprehension of the considered aspect is of significance for *FE* simulation of behavior of active/adaptive structures as well as implementation and test of control algorithms. The assessment

of developed control algorithms through *FEM* simulations may be notably affected by this aspect, especially if not enough care is taken when meshing the structure, e.g., if automatic meshers had been used without further checks on quality of the mesh. As demonstrated, the sensor function of active elements combined with predefined displacements as a part of mechanical excitation is expected to be most critical regarding the aspect. It is advised to invest additional effort in meshing in order to get as uniform mesh over piezopatches as possible. If a distorted mesh is inevitable, one should consider techniques to mitigate the effect of mesh distortion. It was shown that the uniformly reduced integration has offered a significant improvement. Although the advantage offered by the approach has been demonstrated only in the aforementioned critical case, it should be emphasized that it also had a positive influence in all the considered cases. On the other hand, the technique comes with the drawback of possible occurrence of zero-energy modes. Although the application of the full biquadratic shell element gives rise to zero-energy modes only in some quite rare cases (as opposite to a bilinear element), this fact requires caution when the technique is applied. A stabilization of zero-energy modes can be a solution for those cases.

Finally, the presented investigation is done by means of the developed displacement-based shell finite element and the nature of the conclusions is representative for the elements using displacement-based formulation. However, the conclusions cannot be extended to elements based on hybrid formulations and an additional investigation would be necessary to gain worthwhile knowledge about behavior of *FEM* models using this type of elements with respect to the effect of mesh distortion.

Acknowledgements

This paper is supported by the Ministry of Science and Technological Development of Republic of Serbia, Project Nr. TR35005.

References

- Ahmad, S., Irons, B.M. and Zienkiewicz, O.C. (1970), "Analysis of thick and thin shell structures by curved finite elements", *Int. J. Numer. Meth. Eng.*, **2**(3), 419-451.
- Benjeddou, A. (2000), "Advances in piezoelectric finite element modeling of adaptive structural elements: a survey", *Comput. Struct.*, **76**(1-3), 347-363.
- Benjeddou, A., Deü, J.F. and Letombe, S. (2002) "Free vibrations of simply-supported piezoelectric adaptive plates: an exact sandwich formulation", *Thin. Wall. Struct.*, **40**(7), 573-593.
- Gandhi, M.V. and Thompson, B.S. (1992), *Smart materials and structures*, Chapman and Hall, London.
- Hwang, W.S. and Park, H.C. (1993), "Finite element modeling of piezoelectric sensors and actuators", *AIAA J.*, **31**(5), 930-937.
- Klinkel, S. and Wagner, W. (2006), "A geometrically non-linear piezoelectric solid shell element based on a mixed multi-field variational formulation", *Int. J. Num. Meth. Eng.*, **65**(3), 349-382.
- Lammering, R. (1991), "The application of a finite shell element for composites containing piezo-electric polymers in vibration control", *Comput. Struct.*, **41**(5), 1101-1109.
- Liu, G.R., Dai, K.Y., Lim, K.M. and Gu, Y.T. (2002) "A point interpolation mesh free method for static and frequency analysis of two-dimensional piezoelectric structures", *Comput. Mech.*, **29**(6), 510-519.
- Liu, G.R., Dai, K.Y., Lim, K.M. and Gu, Y.T. (2003), "A radial point interpolation method for simulation of twodimensional piezoelectric structures", *Smart Mater. Struct.*, **12**(2), 171-180.
- Liu, G.R., Dai, K.Y. and Nguyen, T.T. (2007), "Theoretical aspects of the smoothed finite element method

- (SFEM)", *Int. J. Num. Meth. Eng.*, **71**(8), 902-930.
- Long, C.S., Loveday, P.W. and Groenwold, A.A. (2006), "Planar four node piezoelectric elements with drilling degrees of freedom", *Int. J. Num. Meth. Eng.*, **65**(11), 1802-1830.
- Marinkovic, D. (2007), *A new finite composite shell element for piezoelectric active structures*, Ph.D. Thesis, Otto-von-Guericke Universitaet Magdeburg, Germany, Fortschritt-Berichte VDI, Reihe 20: Rechnerunterstuetzte Verfahren, Nr. 406, Duesseldorf.
- Marinkovic, D., Koepe, H. and Gabbert, U. (2006), "Numerically efficient finite element formulation for modeling active composite laminates", *Mech. Adv. Mater. Struct.*, **13**, 379-392.
- Marinkovi, D., Köppe, H. and Gabbert, U. (2007), "Accurate modeling of the electric field within piezoelectric layers for active composite structures", *Int. J. Intell. Mater. Syst.*, **18**(5), 503-513.
- Marinkovi, D., Köppe, H. and Gabbert U. (2009), "Aspects of modeling piezoelectric active thin-walled structures", *Int. J. Intell. Mater. Syst.*, **20**(15), 1835-1844.
- Nguyen-Van, H., Mai-Duy, N. and Tran-Cong, T. (2008), "Analysis of piezoelectric solids with an efficient nodebased smoothing element", *Proceedings of the WCCM8 and ECCOMAS 2008*, Venice, Italy.
- Ohs, R.R. and Aluru, N.R. (2001), "Meshless analysis of piezoelectric devices", *Comput. Mech.*, **27**(1), 23-36.
- Rudolf, C., Martin, T. and Wauer, J. (2010), "Control of PKM machine tools using Piezoelectric self-sensing Actuators on basis of the functional principle of a scale with a vibrating string", *Smart Struct. Syst.*, **6**(2), 167-182.
- Sze, K.Y. and Pan, Y.S. (1999), "Hybrid finite element models for piezoelectric materials", *J. Sound Vib.*, **226**(3), 519-547.
- Tzou, H.S. and Tseng, C.I. (1990), "Distributed piezoelectric sensor/actuator design for dynamic measurement/control of distributed parameter systems: a finite element approach", *J. Sound Vib.*, **138**, 17-34.
- Ye, L., Lin, Y., Dong, W., Limin, Z. and L, C. (2010), "Piezo-activated guided wave propagation and interaction with damage in tubular structures", *Smart Struct.Syst.*, **6**(7), 835-849.
- Zemčík, R., Rolfes, R., Rose, M. and Tessler, J. (2006), "High-performance 4-node shell element with piezoelectric coupling", *Mech. Adv. Mater. Struct.*, **13**, 393-401.